Pergamon

Geochimica et Cosmochimica Acta, Vol. 67, No. 19, pp. 3547–3557, 2003

0016-7037/03 $30.00 + .00

doi:10.1016/S0016-7037(03)00212-6

Selenium speciation and partitioning within *Burkholderia cepacia* biofilms formed on α-Al_2O_3 surfaces

ALEXIS S. TEMPLETON,[†1,*] THOMAS P. TRAINOR,[2] ALFRED M. SPORMANN,[3] and GORDON E. BROWN, JR.[1,4]

[1]Surface and Aqueous Geochemistry Group, Department of Geological and Environmental Sciences, Stanford University, Stanford, CA 94035-2115, USA
[2]Consortium for Advanced Radiation Sources, University of Chicago, Chicago, IL 60439, USA
[3]Department of Civil and Environmental Engineering, Stanford University, Stanford, CA 94305, USA
[4]Stanford Synchrotron Radiation Laboratory, SLAC, MS 99, 2575 Sand Hill Road, Menlo Park, CA 94025, USA

(*Received July* 11, 2002; *revised November* 4, 2002; *accepted in revised form January* 9, 2003)

Abstract—The distribution and speciation of Se within aerobic *Burkholderia cepacia* biofilms formed on α-Al_2O_3 (1-102) surfaces have been examined using grazing-angle X-ray spectroscopic techniques. We present quantitative information on the partitioning of 10^{-6} M to 10^{-3} M selenate and selenite between the biofilms and underlying alumina surfaces derived from long-period X-ray standing wave (XSW) data. Changes in the Se partitioning behavior over time are correlated with microbially induced reduction of Se(VI) and Se(IV) to Se(0), as observed from X-ray absorption near edge structure (XANES) spectroscopy.

Selenite preferentially binds to the alumina surfaces, particularly at low [Se], and is increasingly partitioned into the biofilms at higher [Se]. When *B. cepacia* is metabolically active, *B. cepacia* rapidly reduces a fraction of the SeO_3^{2-} to red elemental Se(0). In contrast, selenate is preferentially partitioned into the *B. cepacia* biofilms at all [Se] tested due to a lower affinity for binding to the alumina surface. Rapid reduction of SeO_4^{2-} by *B. cepacia* to Se(IV) and Se(0) subsequently results in a vertical segregation of Se species at the *B. cepacia*/α-Al_2O_3 interface. Elemental Se(0) accumulates within the biofilm with Se(VI), whereas Se(IV) intermediates preferentially sorb to the alumina surface.

B. cepacia/α-Al_2O_3 samples incubated with SeO_4^{2-} and SeO_3^{2-} when the bacteria were metabolically active result in a significant reduction in the mobility of Se vs. X-ray treated biofilms. Remobilization experiments show that a large fraction of the insoluble Se(0) produced within the biofilm is retained during exchange with Se-free solutions. In addition, Se(IV) intermediates generated during Se(VI) reduction are preferentially bound to the alumina surface and do not fully desorb. In contrast, Se(VI) is rapidly and extensively remobilized. *Copyright © 2003 Elsevier Ltd*

1. INTRODUCTION

Selenium contamination of soils, groundwater, and surface waters poses a serious environmental problem in numerous regions globally (e.g., Kesterson Reservoir, CA). The bioavailability of Se is strongly dependent upon its chemical speciation, due to variations in the solubility, mobility, sorptive properties, and uptake mechanisms for each oxidation state of Se. Extensive research on selenium interactions with plants, fungi, bacteria, and soil systems has shown that the biogeochemical cycling of selenium in the environment is largely regulated by micro-scale changes in redox conditions (Frankenberger and Benson, 1994; Frankenberger and Engberg, 1998). Se bioavailability is reduced by the removal of Se via volatilization of biomethylated selenium species (Terry and Zayed, 1994) or via immobilization of Se by precipitation as sparingly soluble, elemental selenium under reducing conditions (Maiers et al., 1988; Oremland, 1994; Tokunaga et al., 1996). Many plants and microorganisms also biochemically assimilate Se (Milne, 1998). Sorption of selenium oxoanions to reactive mineral phases such as metal-(hydr)oxide and clay surfaces may also be an important process for sequestering mobile, dissolved Se species (Balistrieri and Chao, 1987; Neal and Sposito, 1989). For example, selenite (SeO_3^{2-}) sorbs strongly to (hydr)oxide surfaces, and X-ray absorption spectroscopic data indicate the formation of inner-sphere complexes with hydrous aluminum, manganese and iron oxides and clays (Hayes et al., 1987; Foster, 1999; Foster et al., 2003). However, selenate (SeO_4^{2-}) exhibits a low affinity for binding to Al- and Fe-(hydr)oxide surfaces and can be easily remobilized by changes in solution variables such as ionic strength (Davis and Kent, 1990).

The aqueous, chemical reduction of selenate is slow, although rapid surface-catalyzed reduction of selenate can occur via reduction by mixed-Fe(II)Fe(III) minerals such as green rust (Myeni et al., 1997). Microbial organisms play a major role in selenium cycling by catalyzing the reduction of selenate and selenite under anoxic conditions. Numerous organisms have been identified that can reduce SeO_4^{2-} and SeO_3^{2-} to elemental Se(0) (Lortie et al., 1992; Tomei et al., 1992; Garbisu et al., 1996; Milne, 1998; Kessi et al., 1999; De Souza et al., 2001; Roux et al., 2001), as well as to organic forms, such as selenomethionine and selenocysteine (Turner et al., 1998; Van Fleet-Stalder et al., 2000). A few organisms have been isolated that are capable of using selenate or selenite as a terminal electron acceptor (Macy et al., 1989; Oremland et al., 1989; Oremland et al., 1994; Switzer-Blum et al., 1998), and it has been proposed that microbial respiration of selenium oxoanions

* Author to whom correspondence should be addressed (atempleton@ucsd.edu).
† *Present address:* Scripps Institution of Oceanography, Marine Biology Research Division, University of California–San Diego, 9500 Gilman Drive, La Jolla, CA 92093-0202

may be the dominant mode of selenium reduction in sediments (Oremland, 1994).

Monitoring changes in selenium partitioning and speciation in soils and aquatic systems is difficult due to the complexity and heterogeneity of these systems. Therefore, the relative importance of microbial oxidation-reduction reactions vs. sorption processes in the immobilization of Se has been difficult to determine. X-ray absorption spectroscopy (XAS) has proven to be an invaluable tool for probing selenium speciation in sediments from localities such as Kesterson Reservoir (Pickering et al., 1995; Tokunaga et al., 1996) and for determining the mode of Se sorption to reactive surfaces (Hayes et al., 1987; Foster et al., 2002). In this study, we have used X-ray standing wave (XSW) and grazing-incidence X-ray absorption near edge structure (XANES) spectroscopy methods to examine the spatial distribution and speciation of Se, respectively, at the interface between Se-reducing microorganisms and aluminum oxide surfaces the bacteria have colonized (i.e., at the biofilm/mineral interface). We have grown biofilms of *Burkholderia cepacia*, a gram-negative bacterium commonly found in soil environments, on α-Al_2O_3 (1-102) single-crystal substrates, which serve as a chemical and structural analog for Al-(hydr)oxide phases common in soil and aquatic systems. This relatively simple type of biofilm-mineral assemblage was used successfully to investigate Pb(II) partitioning between similar *Burkholderia cepacia* biofilms and α-Al_2O_3 (0001), α-Al_2O_3 (1-102), and α-Fe_2O_3 (0001) substrates (Templeton et al., 2001). The data presented in Templeton et al. (2001) demonstrate that the formation of a *B. cepacia* biofilm does not passivate the intrinsic reactivity of the underlying metal–oxide substrates in the systems studied. In this work, a similar approach, based on the long-period XSW technique, has been used to quantitatively compare the partitioning of both SeO_4^{2-} and SeO_3^{2-} oxoanions at the biofilm/alumina interface. To resolve variations in oxidation state of Se across the biofilm/alumina interface, and to monitor changes in Se speciation as a function of time at various positions relative to this interface, the XSW technique has been coupled with high-resolution XANES spectroscopy at the Se K-edge in the grazing incidence mode.

Experiments were carried out with biofilms of *Burkholderia cepacia* directly transferred from growth media (defined as "active") to solutions varying in Se concentration, initial Se speciation (e.g., SeO_4^{2-}, or SeO_3^{2-}), or exposure time (0.25 h to 1000 h). Parallel experiments were conducted with similar biofilm/alumina samples exposed to X-rays at 14 KeV for 5 min (defined as metabolically "inactive") to measure passive Se sorption processes occurring at reactive surface functional groups present within the biofilm vs. the alumina surface. These X-ray treated samples are also used as a control to identify changes in the partitioning behavior of Se that occur as a result of redox transformations induced by *B. cepacia* in the metabolically active biofilms. The concentration range of the Se amendments was approximately 0.1 to 100 ppm to simulate environmentally relevant [Se].

The spectroscopic data show that SeO_3^{2-} exhibits a much greater affinity for the alumina surface, even in the presence of the *B. cepacia* biofilm, whereas SeO_4^{2-} accumulates within the biofilms. In addition, metabolically active *B. cepacia* catalyzes the rapid reduction of both SeO_4^{2-} and SeO_3^{2-} to Se(0) under aerobic conditions, presumably as a detoxification mechanism. Due to these combined bioreduction and sorption processes, we demonstrate that a segregation of selenium species (i.e., Se(VI) vs. Se(IV) vs. Se(0)) occurs at the biofilm/alumina interface, which has a strong impact on the potential for remobilization of selenium.

2. MATERIAL AND METHODS

2.1. Sample Preparation

Highly polished, 3″-diameter, single crystal α-Al_2O_3 substrates cut parallel to the (1-102) surface (Saint-Gobain Crystals and Detectors) were obtained commercially and subsequently cut into wafers 1 cm wide $\times$ 7 cm long. All wafers were washed in 10^{-2} M nitric acid followed by multiple rinses with MilliQ water and baked at 350°C for 4 h before use. The crystals were characterized by X-ray photoelectron spectroscopy (Surface Science S-Probe, monochromatic Al K_α radiation) before reaction and were found to have no metal contamination on the surfaces. Twenty similar crystals were then attached to polycarbonate coupons and inserted into a jacketed, 900-mL internal-volume annular reactor (Biosurface Technologies) equipped with ports for the introduction and removal of media. After sterilization of the reactor and all media feeds and tubing, a culture of *Burkholderia cepacia* (ATCC 17616) in exponential growth phase in minimal medium was introduced into the main chamber of the reactor. After 24 h in batch-mode, fresh medium was added to the reactor at a rate of 40 mL/h. The inner drum holding the crystals and coupons was rotated at 50 rpm, and temperature was maintained at 30°C. The *B. cepacia* biofilms were grown aerobically over the course of 1 week using a minimal medium (200 μM $CaCl_2$, 150 μM $MgSO_4$, 90 μM $(NH_4)_2SO_4$, 150 μM KNO_3, 10 μM $NaHCO_3$, 5 μM KH_2PO_4, and 100 μM sodium acetate as a carbon and energy source) at pH 6 at an average $O.D._{600}$ of ~0.1. After 1 week, three test crystals were extracted and visualized using either (1) a JEOL JSM-5600LV scanning electron microscope at 15 KeV accelerating voltage to examine the cell density and distribution on the crystal surfaces (Fig. 1) or (2) incubated with a Live/Dead stain (Molecular Probes, Inc.) to visualize the total number of cells on the crystal surface using a Nikon E6000 epifluorescent microscope. All three crystals were extensively colonized by *B. cepacia*, which forms relatively monolayer biofilms, and greater than 90% of the total cells were green (live) vs. red (dead).

Aqueous solutions of selenate and selenite were prepared using reagent grade Na_2SeO_4 and Na_2SeO_3 salts (Sigma) in 18MΩ Barnstead water. The pH was adjusted to 4.5 (where we expect a high level of sorption to the bacterial and alumina surfaces) using 0.1 to 0.01 mol/L HNO_3. The ionic strength of all samples was adjusted to approximately 0.001 mol/L by addition of variable volumes of 1.0 mol/L $NaNO_3$ solution. For experiments with X-ray treated ("inactive") *B. cepacia* biofilms, biofilm-coated crystals were extracted from the reactor, rinsed in fresh media, and exposed to synchrotron X-rays tuned to 14 keV for 5 min before equilibration with Se-bearing solutions. For all other experiments, the crystals were extracted, rinsed in fresh media, and directly immersed in a sterile tub containing 100 mL of a 10^{-6} M to 10^{-3} M aqueous selenate or selenite solution. Samples were equilibrated with the Se-containing solutions for 18 h for fixed-exposure experiments or for 0.25 h up to 1000 h for time-course experiments (biofilm density remains relatively constant). After the selected equilibration period, each crystal was carefully withdrawn from solution under a jet of N_2 to remove bulk water and inserted into a Teflon cell with a Kapton lid attached to the Stanford Synchrotron Radiation Laboratory (SSRL) grazing incidence apparatus. The atmosphere within the Teflon cell was continuously purged with humidified N_2. The [Se] of the solutions was measured before and after equilibration with the biofilm-coated alumina samples using inductively coupled plasma–atomic emission spectrometry. Due to the excess of solution, the uptake of Se had a negligible effect on the solution [Se].

2.2. Data Collection

XSW measurements were conducted on beamline 11-2 at the Stanford Synchrotron Radiation Laboratory using the SSRL grazing incidence apparatus and a 30-element Ge array detector (Canberra) coupled

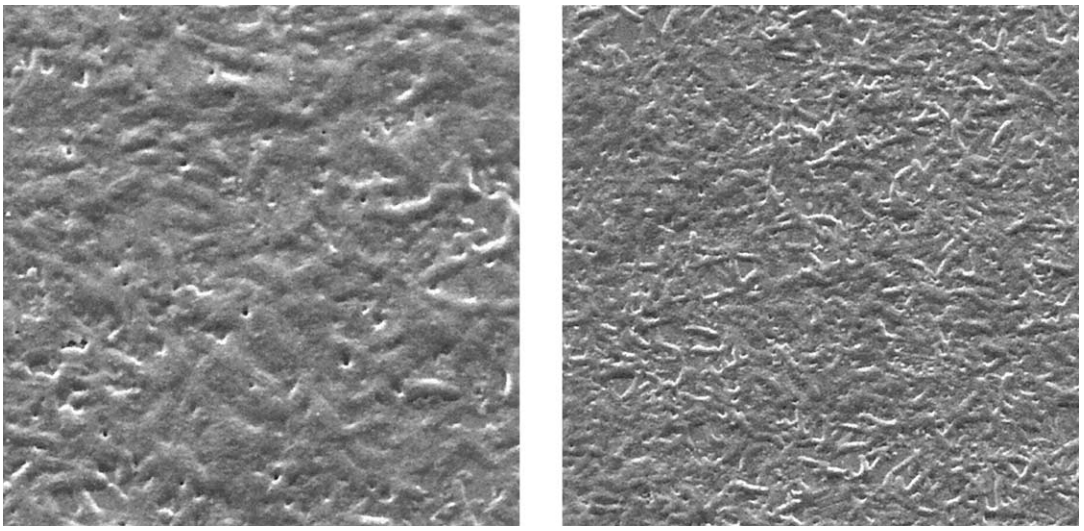

Fig. 1. SEM pictures of *B. cepacia* biofilm on α-Al_2O_3 (1-102). Panel A, where the bacteria are almost entirely encased in an exopolysaccharide matrix, is typical of most regions on most crystals. Panel B shows a more sparsely populated region on the crystal surface where the individual bacteria can be visualized.

to digital X-ray processor (DXP) electronics (X-ray Instrumentation Associates). The incident, unfocused X-rays were monochromatized using a N_2-cooled Si(220) double crystal monochromator. Horizontal and vertical slits before I_o were set at 5 mm and 0.05 mm, respectively. XSW data were collected with 13.5 keV incident X-rays by scanning the incidence angle in step sizes of 5 mdeg from 0 to 400 mdeg. The reflectivity data (Log I_1/I_o) were collected using ionization chambers filled with 10% Ar in He carrier-gas. The Se K_α fluorescent yield (FY) data were collected with a Ge detector aligned 90° to the incident beam and positioned so that all 30 elements view the entire illuminated area on the sample through the scan range. The Se FY profiles were generated by integrating the Se K_α fluorescence peak in the emission spectrum, collected at each incidence angle, followed by background subtraction and normalization relative to I_o. Scatter contributions in the fluorescence windows were removed by fitting the fluorescent lines using a gaussian function and either a linear or Voigt function background to fit the tail of the scatter peak (Trainor et al., 2002b).

XANES spectra were collected using a fixed incident angle and scanning the X-ray energy through the Se K-edge in 0.2-eV steps. The effective energy resolution calculated from the vertical divergence of the beam was approximately 1 eV. Data were collected at two angles to differentiate between the speciation of Se in the biofilm layer vs. Se sorbed to the alumina surface (discussed below). At each angle, four replicate scans of the Se K-edge absorption spectra were collected from 12,400 eV to 12,800 eV and averaged together. The spectra were background subtracted and normalized to the high-energy end of a spline fit through the data. Energy calibration was maintained by collecting a spectrum of a hexagonal elemental Se foil, with the first inflection point taken to be 12,658 eV, before collecting each set of XANES spectra for the biofilm/alumina samples at 50 and 150 mdeg. Spectra of Se references (aqueous selenate and selenite, as well as selenomethionine, selenocysteine, and red elemental selenium) were also collected for comparison to the sample spectra. No evidence of X-ray beam induced reduction of Se was found in any of the model compounds.

Se extended X-ray absorption fine-structure spectroscopy (EXAFS) data were collected in addition to Se K-edge XANES for two samples by scanning in energy above the Se K-edge to approximately 13,650 eV, in 0.5 $Å^{-1}$ steps at 2–10 s per step. Eight scans were averaged together, background subtracted, and normalized using a spline function with 3 nodes. E_0 was designated as 12,675 eV. Fourier transforms of the k^3-weighted EXAFS spectra were derived over the k-range ~3 $Å^{-1}$ to 12 $Å^{-1}$ and were not corrected for phase-shift. Therefore, the true radial distances are approximately 0.3 to 0.5 Å longer than shown in the FT. Structural fitting of the EXAFS spectra was not conducted.

2.3. Data Analysis

The reflectivity (Log I_1/I_0) data were modeled for each sample to obtain the density and roughness of the biofilm layer. Reflectivity was calculated using the optical recursion formula (Parratt, 1954) with refractive indices for the alumina and biofilm layers calculated using the absorption code of Brennan and Cowan (1992). An empirical damping factor, similar to a Debye-Waller-type term, was included in the calculation of the reflection coefficients to account for interfacial roughness. In the fits, the biofilm layer thickness was fixed at 10,000 Å (monolayer biofilm approximately 1 μm thick), and extracted values for the biofilm densities and biofilm-layer roughness for these *ex situ* samples ranged from 0.2 to 0.85 g/cm^3 and 50 to 200 Å, respectively.

The fluorescence yield data were subsequently modeled using Eqn. 1 (Abruna et al., 1990; Bedzyk et al., 1990; Bommarito et al., 1990),

$$Y(\theta) \propto \int N(z)\, I(z,\theta) dz \tag{1}$$

where N(z) is the distribution function of the fluorescing species (i.e., Se) and the intensity modulation of the XSW field above the crystal surface is calculated from Eqn. 2.

$$I_{xsw} = |E_i(z,\theta) + E_r(z,\theta)|^2 \tag{2}$$

In Eqn. 2 $E_i(z,\theta)$ and $E_r(z,\theta)$ are the complex amplitudes of the incident and reflected beams, respectively (Parratt, 1954; Krol et al., 1988; De Boer, 1991) and result from modeling the reflectivity data as discussed above (see Trainor, 2001). The standing wave period varies from >1000 Å at low angles to D_c, where D_c is the standing wave period at the critical angle of the substrate (D_c is ~159 Å for α-Al_2O_3).

The vertical (z) Se distribution function used to calculate the fluorescence yield in Eqn. 1 is a discontinuous, two-box model

$$N(z) = \begin{cases} N_{alumina} & 0 \le z \le z_{min} \\ N_{biofilm} & z_{min} < z < 10{,}000 Å \end{cases} \tag{3}$$

where $N_{biofilm}$ is the bulk [Se] in the biofilm and $N_{alumina}$ is the adsorbed [Se] at the alumina surface. The thickness of the "alumina" layer (z_{min}) was designated as 5 Å for all calculations.

For a layer of Se atoms at position z ($N_{(z)}$), the Se fluorescence intensity is proportional to the standing wave intensity (I_{xsw}) at position z (De Boer, 1991). The calculations take into account attenuation of I_{xsw} and escaping fluorescent X-rays within the biofilm as well as changes in the illuminated area of the sample as the incident angle is

scanned from 0 mdeg to 400 mdeg. (Trainor, 2001). The final calculated yield profiles were convolved with a gaussian resolution function with a full width at half-maximum of approximately 25 mdeg.

A least-squares routine was applied to fit the Se K_α fluorescence yield data between 0.04 and 0.4 deg. The total [Se] in the alumina surface and the biofilm layer was varied to simulate the fluorescence yield profiles (reported as a surface:biofilm ratio, S/B). The S/B ratios have a precision of ±10% within the useful range of 20 to 0.05. The most sensitive parameter in determining the relative FY intensities at approximately 50 mdeg vs. 150 mdeg is the ratio of the surface-to-biofilm bound Se (i.e., S/B ratio). In the profiles collected in this study, there is insufficient fine structure in the total FY profile to differentiate between a heterogeneous vs. homogeneous vertical distribution of Se, so an average [Se] is used in the modeling.

The speciation of Se in the biofilm vs. the alumina surface can be differentiated by scanning in energy at a fixed incidence angle of 50 mdeg to obtain Se-biofilm dominated XANES and then at 150 mdeg, which is just below the critical angle for the α-Al_2O_3 substrate, to obtain XANES spectra dominated by Se at the alumina surface. At 50 mdeg, 99% of the fluorescence signal is derived from Se atoms residing at positions above the oxide surface (i.e., in the biofilm). At 150 mdeg, the fraction of Se fluorescence derived from biofilm Se vs. alumina Se must be determined from the S/B partitioning ratios obtained from the XSW spectra. For example, at a S/B ratio of 2, ~75% of Se fluorescence collected at 150 mdeg is derived from Se atoms bound to the oxide surface. For a S/B ratio of 1, ~65% of the Se fluorescence is derived from Se atoms in the 5Å mineral surface layer, and for a S/B ratio of 0.5, only ~50% of the Se fluorescence at 150 mdeg is associated with the alumina surface.

Se XANES spectra were curve-fit between 12,640 and 12,700 eV using a linear-combination fitting procedure in DATFIT, which is part of the EXAFSPAK suite of programs (George and Pickering, 1995). The mole fraction of a given selenium species/model compound present in the sample can be determined directly by its fractional contribution of the fit of the unknown XANES spectrum (Pickering et al., 1995; Pickering et al., 2000). The suite of selenium model compounds used in the fitting procedure included selenomethionine, selenocysteine, red elemental selenium, aqueous selenite, and aqueous selenate, although the abundance of the organo-selenium compounds (selenomethionine and selenocysteine) in the unknown spectra was typically not above the detection limit (~5%). The quality of the fits (determined by minimizing the residual of the fit; χ^2) for the XANES spectra is very good at high [Se] and only slightly poorer at lower [Se] (i.e., 10^{-5}M or "residual" samples), where the signal-to-noise ratio of the data is diminished. A minimal energy offset for the model spectra was allowed during the fitting procedure, and was always observed to be less than 0.3 eV. The sum of all model spectra used to fit each unknown XANES spectra was within ±0.05 U of unity.

3. RESULTS

3.1. Selenite and Selenate Sorption to X-ray Treated (Inactive) *B. cepacia*/α-Al_2O_3

XSW FY profiles were collected for both selenite and selenate sorbed to X-ray treated (inactive) *B. cepacia* biofilms formed on the α-Al_2O_3 (1-102) surfaces to quantitatively determine the partitioning of Se(IV) and Se(VI) species between the biofilm and the underlying mineral surface. The data can be used to track changes in the partitioning of SeO_3^{2-} or SeO_4^{2-} over a large range in [Se], as well as to directly compare the sorption behavior of Se(IV) vs. Se(VI) species, under conditions where only passive sorption is expected to occur.

In Figure 2a, FY profiles for samples equilibrated with 10^{-6} M to 10^{-3} M Na_2SeO_3 solutions (pH 4.5) for 18 h are shown. At 10^{-6} M SeO_3^{2-}, the FY profile is sharply peaked towards the critical angle (~155mdeg), which indicates that selenite is preferentially bound to the alumina surface and little selenite can be detected within the overlying biofilm. At increasing

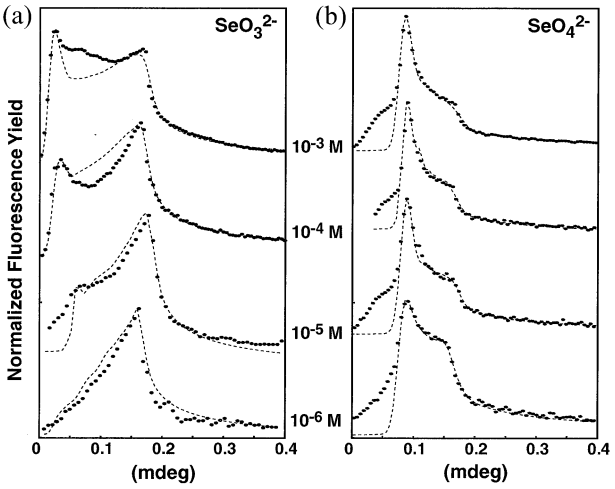

Fig. 2. Se fluorescence yield (FY) as a function of X-ray incidence angle (θ) for 10^{-6} M to 10^{-3} M SeO_3^{2-} and SeO_4^{2-} sorbed to X-ray treated *B. cepacia* biofilms formed on α-Al_2O_3 (1-102) surfaces. Data are shown as closed circles, fits for Figure 3A as dashed lines. FY at the critical angle (~155 mdeg) is largely due to Se ions associated with the alumina surface, whereas FY at lower angles (i.e., 50 mdeg) is indicative of Se ions residing above the surface (i.e., in the biofilm).

SeO_3^{2-} concentrations, there is a systematic increase in the relative FY observed at low angles (i.e., 50 mdeg), indicating enhanced selenite uptake by the biofilm at higher [SeO_3^{2-}]. At the highest SeO_3^{2-} concentration tested (10^{-3} M), the relatively flat-topped FY profile indicates that selenite is almost equally partitioned between the alumina surface and the biofilm (Fig. 2a).

The FY profiles obtained for Se(VI) species sorbed to the *B. cepacia*/α-Al_2O_3 samples differ significantly from the Se(IV) profiles (Fig. 2b). At the lowest SeO_4^{2-} concentration tested (10^{-6} M), Se(VI) species are preferentially partitioned into the biofilm vs. the alumina surface (S/B ~0.25). As the SeO_4^{2-} concentration is increased by an order of magnitude, the increasing maxima in the FY profiles at low angles (i.e., 50 mdeg) indicate that the biofilm forms the dominant sink for SeO_4^{2-}.

Modeling of the FY profiles using a two-box model (mineral surface vs. biofilm layer) was performed to obtain a ratio of surface-bound Se to biofilm-bound Se (reported as a S/B ratio) at each [Se] examined. Fits of the FY profiles are overlain on the data shown in Figures 2a and 2b, and a quantitative comparison of the Se(IV) and Se(VI) partitioning behavior for the X-ray treated samples is shown in Figure 3A. For both Se(IV) and Se(VI) species, the largest S/B ratios are obtained at the lowest [Se] (10^{-6} M), which indicates preferential binding to sites on the alumina surface. At higher [Se], there is a systematic decrease in the S/B ratios as the biofilm becomes a more important sink for Se. At each [Se], the S/B ratios obtained for Se(IV) are 1–2 orders of magnitude larger than Se(VI) species under the same conditions, indicating a much greater affinity of Se(IV) than Se(VI) for the alumina surface. Two lines of evidence suggest that the difference in the partitioning behavior cannot be attributed to preferential binding of Se(VI) to the biofilm. First, the total FY measured at low angles (i.e., FY derived from the biofilm) was approximately equivalent for

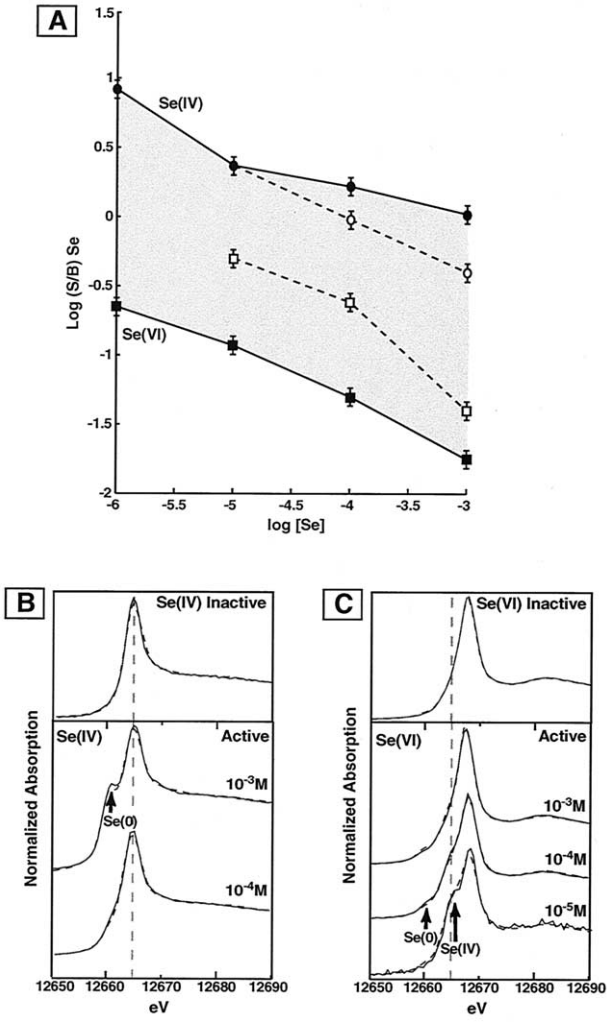

Fig. 3. (A) Log partition ratios (alumina surface-bound Se/biofilm-bound Se, reported as S/B ratio) vs. log [Se] obtained for selenite (circles) and selenate (squares) sorbed to biofilm-coated α-Al_2O_3 (1-102). S/B ratios for both metabolically active (open) and X-ray treated (filled) *B. cepacia* biofilms incubated with 10^{-6} M to 10^{-3} M Se are shown. The S/B ratios are derived from fitting FY profiles using a two-box model, as shown in Figure 2. (B) Se K-edge XANES collected at 50 mdeg (biofilm-sensitive) for selenite incubated with metabolically active and X-ray treated (inactive) *B. cepacia* biofilms formed on α-Al_2O_3 (1-102) surfaces. XANES spectra were collected with the Se FY profiles used to obtain each S/B ratio presented in (A). Linear-combination fits of each XANES spectra, which include varying fractions of selenate, selenite, and (red) elemental Se, are shown (dashed lines). Fractions of each model compound used in each XANES fit are reported in Table 1. (C) Same construction as (B). Se K-edge XANES collected at 150 mdeg (alumina sensitive) for selenate incubated with metabolically active and X-ray treated (inactive) *B. cepacia* biofilms formed on α-Al_2O_3 (1-102) surfaces.

biofilms equilibrated with 10^{-3} M SeO_4^{2-} or SeO_3^{2-} (data not shown). The magnitude of the FY provides a qualitative comparison of Se uptake, and should differ markedly if significantly greater sorption of Se(VI) occurred. Second, cell suspensions (*B. cepacia* and associated exopolysaccharides) incubated with equimolar concentrations of SeO_3^{2-} or SeO_4^{2-} bound similar amounts of Se (~95 μmol/g vs. 92 μmol/g, respectively at 10^{-4} M [Se]). Instead, the difference in S/B ratios can be primarily attributed to the significantly higher reactivity of SeO_3^{2-} vs. SeO_4^{2-} for the alumina surface.

3.2. Selenium Partitioning at Metabolically Active *B. cepacia*/α-Al_2O_3 Interfaces

FY profiles were obtained for a series of experiments where *B. cepacia* was directly transferred from the growth reactor to SeO_3^{2-} and SeO_4^{2-} solutions ("active"). The FY profiles were also modeled to obtain S/B ratios (Fig. 3A). The S/B ratios can be used to compare the Se partitioning behavior within biofilms, where some fraction of the Se species may undergo oxidation or reduction reactions, to the partitioning behavior measured for the X-ray treated biofilms where only sorption occurs (Fig. 3A). In Figure 3A, the S/B ratios for the metabolically active Se(IV) samples are all shifted to *lower* values than obtained for the X-ray treated experiments (see S/B curves from 10^{-4} M to 10^{-3} M SeO_3^{2-}). In contrast, the S/B ratios for the metabolically active Se(VI) samples are all shifted to *higher* values than obtained for the inactive experiments (see S/B curves from 10^{-5} to 10^{-3} M SeO_4^{2-}).

The underlying causes for the changes in the Se partitioning between the X-ray treated cell vs. active cell experiments can be explained using Se K-edge XANES spectra obtained after collecting each Se FY profile. The energy position of the Se K-absorption edge is particularly sensitive to variations in the redox state of Se (e.g., Se(0), Se(IV), and Se(VI) species are each separated by a few eV). Discriminating between Se(0) and a variety of organic forms of Se, such as selenocysteine and selenomethionine, relies upon differences in the fine-structure above the K-edge, but again the spectra are distinct from each other.

Visual inspection and quantitative fitting of the XANES spectra for SeO_3^{2-} and SeO_4^{2-} sorbed to X-ray treated *B. cepacia*/α-Al_2O_3 samples show that there is no change in selenium oxidation state during sorption of Se to the inactive biofilms or the alumina surface. Representative spectra are shown in the top panels of Figures 3B and 3C. X-ray treated samples incubated with SeO_4^{2-} can be fully described using only the selenate model spectra, and samples reacted with SeO_3^{2-} are well fit using only the selenite model spectra. No evidence for Se reduction was observed for any of the X-ray treated samples. However, there are dramatic changes in selenium oxidation state for Se sorbed to metabolically active biofilms. Quantitative fitting results for the changes in Se speciation for active samples reacted with SeO_3^{2-} and SeO_4^{2-}, derived from the linear-combination fitting of the XANES spectra, are reported in Table 1. For the Se(IV) series, a minor shoulder in the XANES spectra near 12,660 eV for 10^{-4} M SeO_3^{2-} becomes a pronounced shoulder at 10^{-3} M SeO_3^{2-}. This shoulder can be attributed to the reduction of Se(IV) and accumulation of elemental Se(0). For the Se(VI) series, a pronounced shoulder at 12,665 eV in the XANES spectra at 10^{-5} M SeO_4^{2-} indicates the presence of a significant fraction of Se(IV). No Se(IV) species were provided during the incubations; therefore, Se(IV) must have been generated by Se(VI) reduction. At higher SeO_4^{2-} concentrations, a small feature at 12,660 eV also shows the accumulation of a small amount of elemental Se(0).

Table 1. Fits for XANES spectra of SeO_3^{2-} or SeO_4^{2-} incubated with *B. cepacia*/α-Al_2O_3.

$Selenium_{(initial)}$	Treatment	[Se]	Se(VI)	Se(IV)	Se(0)	Residual χ^2
SeO_3^{2-}	X-ray	10^{-6}	—	—	—	No data
SeO_3^{2-}	X-ray	10^{-5}	0.0	1.01	0.0	$0.3e^{-3}$
SeO_3^{2-}	X-ray	10^{-4}	0.0	1.0	0.0	$0.3e^{-3}$
SeO_3^{2-}	X-ray	10^{-3}	0.0	1.01	0.0	$0.2e^{-3}$
SeO_3^{2-}	active	10^{-4}	0.0	0.80	0.20	$0.1e^{-3}$
SeO_3^{2-}	active	10^{-3}	0.0	0.51	0.49	0.5^{e-3}
SeO_4^{2-}	X-ray	10^{-6}	—	—	—	No data
SeO_4^{2-}	X-ray	10^{-5}	0.99	0	0	$0.3e^{-3}$
SeO_4^{2-}	X-ray	10^{-4}	—	—	—	No data
SeO_4^{2-}	X-ray	10^{-3}	1.0	0	0	$0.2e^{-3}$
SeO_4^{2-}	active	10^{-5}	0.63	0.32	0.05	$0.4e^{-3}$
SeO_4^{2-}	active	10^{-4}	0.73	0.21	0.06	$0.5e^{-3}$
SeO_4^{2-}	active	10^{-3}	0.87	0.065	0.065	$0.8e^{-3}$

Se oxidation state (reported as the fraction of Se(VI), Se(IV), and Se(0)) measured for metabolically active and X-ray treated (inactive) *B. cepacia* biofilms grown on α-Al_2O_3 (1-102) incubated with 10^{-6} M to 10^{-3} M Se. The fraction of Se(VI), Se(IV), and red elemental Se(0) were determined using linear-combination fitting of XANES spectra (selenocysteine and selenomethionine were below detection limit for all fits). Spectra and fits are shown in Figs. 3B and 3C.

The differences in selenium speciation for X-ray treated vs. active biofilms (Figs. 3B and 3C) can be used to explain the differences in Se partitioning behavior shown in Figure 3A. For the Se(IV) series, the production of elemental Se(0) by *B. cepacia* lowers the S/B ratios measured at higher SeO_3^{2-} concentration, since the majority of the Se(0) is accumulating within the biofilm rather than at the alumina surface. The vertical segregation of Se(0) and Se(IV) species can be confirmed by comparing XANES measurements collected at low vs. high incident angle. Spectra obtained at 50 mdeg and 150 mdeg are sensitive to the biofilm Se vs. the Se bound to alumina speciation, respectively (see Section 2.3 and the example in Fig. 4). In Figure 3B, the XANES spectrum for 10^{-3} M SeO_3^{2-} shows a strong Se(0) shoulder at 12,660 eV. This feature is much more pronounced at 50 mdeg than at 150 mdeg (data not shown), which implies that the Se(0) resides at positions above the alumina surface (i.e., within the biofilm).

In contrast to the Se(IV) data, the S/B ratios for the metabolically active *B. cepacia*/α-Al_2O_3 samples incubated with SeO_4^{2-} are *higher* than the X-ray treated samples. This implies that a greater fraction of the total Se is associated with the alumina surface. The XANES data shown in Figure 3C indicate that there is significant production of Se(IV), particularly when the samples are amended with low Se(VI) concentrations. We suggest that due to the much higher reactivity of Se(IV) vs. Se(VI) species for the alumina surface, the Se(IV) generated from Se(VI) reduction accumulates at the alumina surface and shifts the S/B ratio to much larger values. This suggestion is supported by comparing the Se speciation in the biofilm vs. that on the alumina surface as shown in Figure 4 for the 10^{-5} M SeO_4^{2-} sample. XANES spectra collected at 150 mdeg (surface sensitive) show a mixture of Se(IV) and Se(VI) species, whereas XANES spectra collected at 50 mdeg (biofilm sensitive) are dominated by Se(VI) and show a small Se(0) shoulder. Therefore, Se(IV) primarily resides at the alumina surface whereas Se(VI) and Se(0) preferentially accumulate in the biofilm. At high SeO_4^{2-} concentrations, the majority of the Se is in the Se(VI) form for the untreated, active samples. Therefore, there is only a small difference in the S/B ratio compared to the X-ray treated sample at 10^{-3} M SeO_4^{2-}.

3.3. Changes in Se(IV) and Se(VI) Speciation Over Time

A series of experiments were conducted with metabolically active *B. cepacia*/α-Al_2O_3 samples which were incubated with 10^{-3} M SeO_3^{2-} and 10^{-4} M SeO_3^{2-} solutions as a function of time immediately after extraction from the biofilm growth

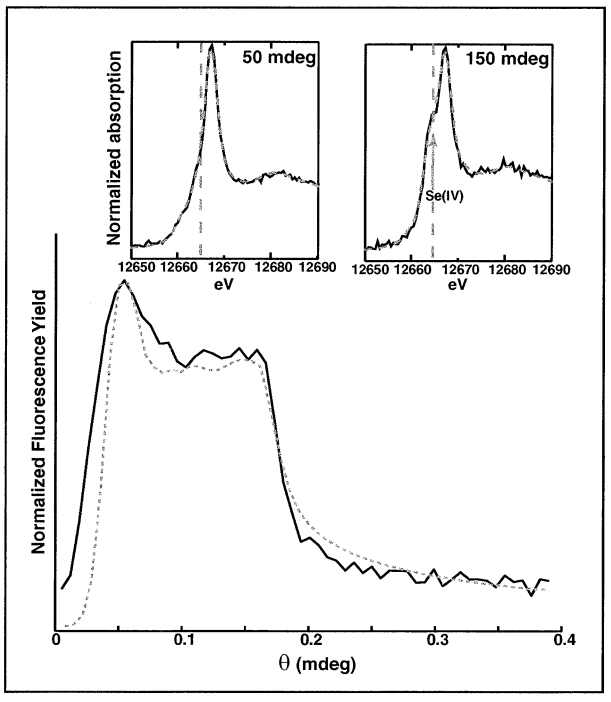

Fig. 4. Example of the differentiation between Se oxidation state in the biofilm vs. the alumina surface for a metabolically active *B. cepacia* biofilm on α-Al_2O_3(1-102) incubated with 10^{-5} M SeO_4^{2-}. The Se FY profile is shown and XANES spectra were collected at 50 mdeg (biofilm-dominated) and 150 mdeg (surface-sensitive). The 50 mdeg spectra is 16% Se(0) and 84% Se(VI). In contrast, the 150 mdeg spectra is 5% Se(0), 32% Se(IV), and 63% Se(VI), demonstrating that Se(IV) preferentially accumulates at the alumina surface after reduction of Se(VI).

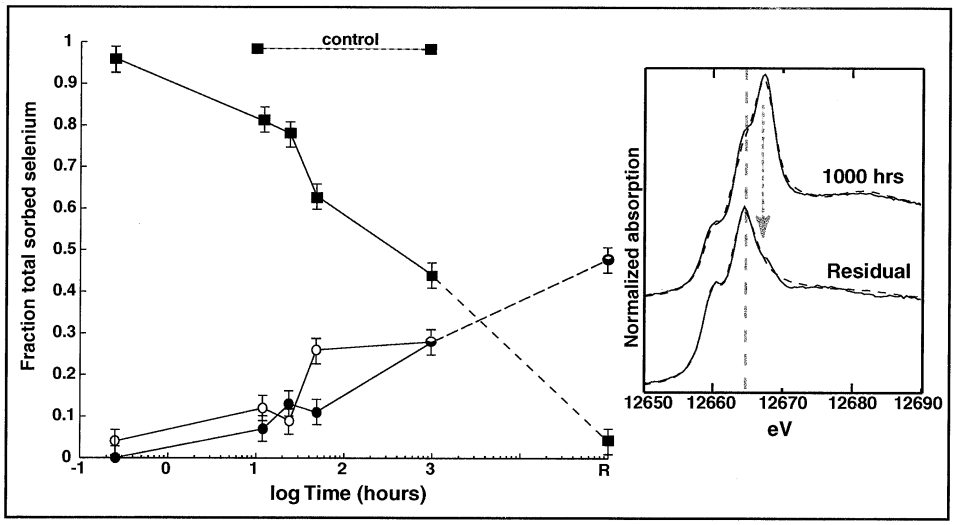

Fig. 5. Sorbed selenium oxidation state vs. time (hours) for selenate incubated with *B. cepacia* biofilms formed on α-Al_2O_3 (1-102) surfaces. The fraction of selenate (squares), selenite (filled circles) and elemental selenium (empty circles) was determined using a linear-combination fitting procedure for XANES spectra collected at 150 mdeg for each time point. The incubation series was conducted from 0.25 to 1000 h. The 1000-h sample was then immersed in 10 mL of Se-free media for 12 h, and XANES spectra were collected to determine the speciation of the residual bound selenium (point R). Inset: XANES spectra for the 1000 h and R (residual after "washing" 1000 h) samples. At 1000 h, there is 44% Se(VI), 28% Se(IV), and 28% Se(0) at 150 mdeg. After remobilization, the Se(VI) has been removed and the residual selenium is 50% Se(IV) and 50% Se(0).

reactor. These respective [Se] were chosen based on the observation of significant changes in 10^{-3} M SeO_3^{2-} and 10^{-4} M SeO_4^{2-} speciation at 18 h in the experiments presented in Figure 3. The fraction of Se species present in each sample was determined using the linear-combination fitting procedure for XANES spectra collected at each time-point. Control experiments conducted in parallel for 18 and 48 h with X-ray treated samples show that no reduction of Se(IV) or Se(VI) occurred.

For Se(IV), experiments with metabolically active *B. cepacia*/alumina samples were conducted from 0.25 to 48 h. Although the SeO_3^{2-} concentration of the solution is unchanged (due to large solution volume relative to sample size), increases in the total Se FY measured over time qualitatively suggest that the total amount of sorbed Se increased through the entire time period. At 0.25 h, only Se(IV) was present in the samples. At 12 h, significant accumulation of Se(0) had occurred (54% of the total Se). The fraction of Se(IV) vs. Se(0) did not change significantly through the rest of the time period. Apparently, selenite first sorbs to the cells (and/or is taken up intracellularly), and the reduction does not begin within the first 15 min; however, by 12 h, the majority of selenium reduction has occurred (data not shown).

For Se(VI), the total Se uptake (qualitatively monitored from the FY) increased throughout at least the first 48 h of the 1000 h time period. Significant changes in Se speciation occurred at each time-point, as shown in Figure 5. At 0.25 h, the majority of Se is Se(VI), with the possible production of small amounts of Se(0) (at the detection limit). Comparison of the selenium oxidation state derived from XANES data at each time point shows a systematic decrease in the fraction of Se(VI) within the active *B. cepacia*/α-Al_2O_3 samples. At time points less than 48 h, there is more Se(0) than Se(IV) in the biofilms, but in general we observe a systematic increase in the fraction of both reduced species. At 1000 h, there is a pronounced accumulation of both Se(0) and Se(IV). The XANES spectrum for 1000 h is shown in the inset of Figure 5

3.4. Se(IV) and Se(VI) Remobilization

To examine the potential changes in Se partitioning that would occur if Se-amended samples were "remobilized" by exposure to Se-free solutions, the 1000 h Se(VI) sample and 48 h Se(IV) sample were reequilibrated with 0.005 mol/L $NaNO_3$ solution for 12 h. This wash procedure resulted in a large reduction of the total Se present in each sample as well as in dramatic changes in the ratios of Se species in each sample. The total FY for the Se(IV) and Se(VI) sample was reduced by 61% and 89%, respectively. For the Se(IV) sample, Se(IV) was preferentially remobilized from the biofilm and retained at the alumina surface. Only Se(0) remained in the biofilm, and Se(IV) was localized to the alumina surface (see Fig. 6). For the biofilm previously reacted with 10^{-4} M SeO_4^{2-} for 1000 h, the Se(VI) was preferentially remobilized, leaving equal proportions of Se(0) and Se(IV). The XANES spectra for the residual Se are shown in the inset to Figure 5. Comparison to the original XANES spectra for the 1000 h sample shows the removal of the Se(VI) peak at 12,668 eV. Interestingly, the residual Se is not entirely in the Se(0) form. The production and accumulation of Se(IV) species during selenate reduction have resulted in significant sequestration of Se (as Se(IV)) at the alumina surface as well as in the relatively immobile and insoluble Se(0) form within the biofilm.

4. DISCUSSION

The XSW profiles obtained for SeO_3^{2-} and SeO_4^{2-} sorption to X-ray treated *B. cepacia*/α-Al_2O_3 (1-102) samples show that

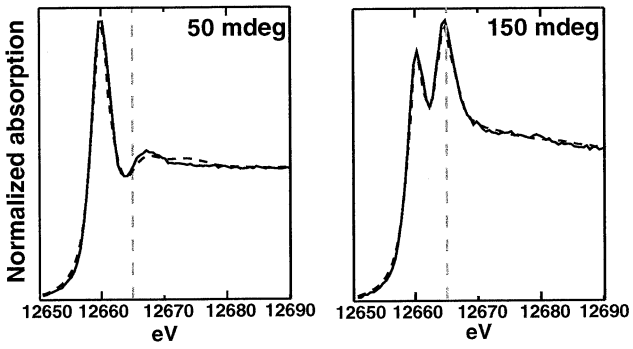

Fig. 6. XANES spectra collected at 50 mdeg and 150 mdeg for the 48 h 10^{-3} M SeO_3^{2-} sample after remobilization by immersion in 10 mL of Se-free solution for 12 h. At 50 mdeg, the XANES spectra are fit by 85% Se(0) and 15% selenomethionine. At 150 mdeg, the XANES are fit by 64% Se(0) and 36% Se(IV). The combined data show that Se(0) is retained within the biofilm, whereas Se(IV) is sequestered at the alumina surface.

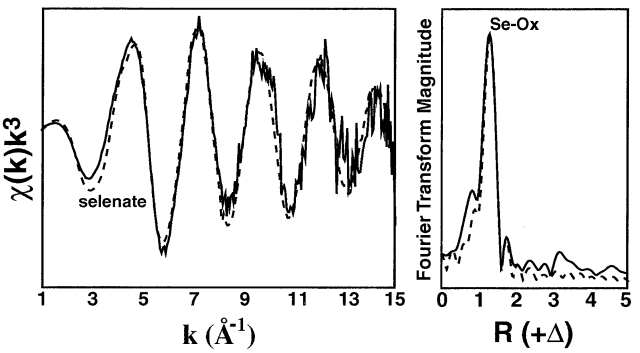

Fig. 7. Se EXAFS and corresponding Fourier transform (solid) for X-ray treated *B. cepacia*/α-Al_2O_3 (1-102) equilibrated with10^{-3} M SeO_4^{2-}, pH 4.5. The EXAFS spectrum is strongly similar to the spectrum collected for an aqueous selenate solution (dashed).

selenite has a much higher affinity for the alumina surface than selenate, even when a biofilm has formed on the alumina surface. At low [Se], SeO_3^{2-} will penetrate the biofilm and preferentially bind to the mineral surface. SeO_4^{2-} also binds to the alumina surface at low [Se] (i.e., 10^{-6} M SeO_4^{2-}), but the total uptake at the alumina surface is not significantly greater than within the biofilm. At higher [Se] the biofilm rapidly becomes the major sink for SeO_4^{2-}. The difference in partitioning behavior for Se(IV) vs. Se(VI) species agrees well with previous (biofilm-free) studies of selenite and selenate sorption onto Al- and Fe-(hydr)oxide surfaces, where selenite has been shown to form stronger surface complexes with surface hydroxyl functional groups (Hayes et al., 1987; Foster, 1999). Although we do not have EXAFS spectra for SeO_4^{2-} sorbed to α-Al_2O_3 (1-102), we would predict that the majority of sorbed SeO_4^{2-} would be outer-sphere complexes, as observed for sorption to clays surfaces (Foster, 1999), although some inner-sphere SeO_4^{2-} complexes may exist where defect sites or singly coordinated surface oxygen atoms will be exposed at the α-Al_2O_3 (1-102) surface (Trainor et al., 2002a). In our previous work on Pb(II) sorption to *B. cepacia* coated metal–oxide surfaces, the formation of the biofilm did not alter differences in the intrinsic reactivity of several different metal–oxide surfaces towards aqueous Pb(II) (Templeton et al., 2001). Therefore, we are not surprised that variations in the behavior of selenite vs. selenate are also preserved on α-Al_2O_3 (1-102).

The significant uptake of selenite and selenate by both the active and the X-ray treated biofilms, especially at high [Se], is particularly intriguing. Although EXAFS spectroscopy was not an integral part of this study, an EXAFS spectrum was collected for the X-ray treated *B. cepacia* sample reacted with 10^{-3} M SeO_4^{2-}, as a preliminary effort to probe the structure of the selenate sorption complexes (Fig. 7). However, this approach was unsuccessful because the EXAFS spectra obtained were so similar to the spectrum collected for aqueous selenate. The spectral match with aqueous selenate suggests the formation of outer-sphere complexes, but may just reflect the weak scattering power of potential backscatterers, such as carbon, phosphorous, or nitrogen derived from bacterial surface functional groups.

Se XSW partitioning data for metabolically active *B. cepacia* biofilms vary significantly from the baseline obtained from the X-ray treated samples. For selenite, the S/B ratios derived from the XSW data are always lower (i.e., more biofilm dominated) due to increased sequestration of selenium, in the form of Se(0), in the biofilms. The XANES data in Figure 3B show that the speciation of selenium in the biofilm differs markedly in the active samples due to the reduction of Se(IV) to elemental Se(0). This is important in terms of increasing total uptake (which is confirmed by measuring an increase in the total FY), as well as altering the speciation, and therefore the remobilization potential, of the Se. In the X-ray treated samples incubated with 10^{-3} M SeO_3^{2-}, the washing procedure removed 80% of the selenium bound to the sample, whereas only 61% was removed for the metabolically active sample. In the X-ray treated sample, the biofilm selenium was preferentially removed, because the biofilm essentially reequilibrated with a solution with a lower [Se], and Se(IV) desorbs more readily from the biofilm because it forms weaker complexes with the bacterial surface functional groups than functional groups on the alumina surface. In contrast, in the active sample the retention of selenium in the biofilm is enhanced, because the production of Se(0) has generated a recalcitrant, sparingly soluble form of Se that remains while the Se(VI) species reenter the solution phase.

The combined XSW partitioning and XANES data for SeO_4^{2-} show that the microbial reduction of selenate generates a mixture of reduced species (Se(IV) and Se(0)) that are segregated at the biofilm/alumina interface. Se(0) is dominantly associated with the biofilm, where reduction must occur (the α-Al_2O_3 surface cannot reduce Se(VI)). Some fraction of the Se(IV), which should be a transient intermediate and cannot be detected in the solution phase, preferentially accumulates at the alumina surface, thereby increasing the S/B ratios. Although Se(VI) is easily removed during exchange with the Se-free solutions, there is a strong hysteresis in Se(IV) desorption and quantitatively, the retention of Se(IV) at the alumina surface is comparable to the retention of Se(0) within the biofilm (e.g., Fig. 5 inset). Similar hysteresis for selenite desorption has been observed in abiotic studies of Se(IV)/Fe–oxide interactions (Zhang and Sparks, 1990; Su and Suarez, 2000). Therefore, there is not significant desorption of Se(IV) from the alumina

surface, and the bioavailability, or susceptibility to bioreduction, of the Se(IV) bound to alumina is unknown.

Indirect estimates of the Se sorption density (μmol Se/m^2 crystal surface area) can be made by comparison of a variety of forms of data collected in the course of our XSW experiments. We have studied selenate sorption onto α-Al_2O_3 (1-102) in biofilm-free systems using the in situ XSW technique and have derived isotherms for selenate uptake (Trainor et al., 2002b). From the isotherms, we can provide surface coverage estimates of approximately 0.4 μmol/m^2 Se(VI) on the surface at $10^{-4.22}$ M SeO_4^{2-} and 2.4 μmol/m^2 Se(VI) at $10^{-3.22}$ M SeO_4^{2-}. Assuming that the formation of the biofilm has not significantly altered the selenate uptake at the mineral surface, these values can be used to approximate a selenium concentration in the X-ray treated biofilms from the S/B ratios. For example, at 10^{-4} M SeO_4^{2-}, the sorbed [Se] at the alumina surface would be 0.65 μmol/m^2 (assuming a linear isotherm), and therefore the Se(VI) in the X-ray treated biofilm would be approximately 12.9 μmol/m^2 (crystal surface-area). A similar calculation cannot be made for the active biofilms because there has been the significant accumulation of Se(IV) species at the alumina surface in addition to Se(VI), so we do not know the baseline Se sorption density.

B. cepacia is tolerant to Se(IV) and Se(VI) oxoanions and will grow in minimal media amended with either 10^{-4} M SeO_4^{2-} or SeO_3^{2-}. In addition, there is no evidence for cell death upon exposure to up to 10^{-3} M SeO_4^{2-} or SeO_3^{2-} from epifluorescent microscopy observations using the Live/Dead stain after the Se-incubations (>90% green [live] in the assay). Reduction of Se oxoanions by *B. cepacia* has not previously been reported, and therefore the production of Se(0) and Se(IV) under aerobic conditions was a new finding in this study. The accumulation of Se(IV) at the alumina surface during the Se(VI) experiments was unexpected. Se(IV) reduction is often observed to be more rapid and more extensive than Se(VI) reduction (Ike et al., 2000). None of the time series data indicates that Se(IV) forms from the reoxidation of Se(0), and red Se(0) is a stable product in *B. cepacia* cell suspensions over the course of months. However, transient accumulation of Se(IV) has been observed during Se(VI) reduction when the Se(VI) reduction rate is much greater than that for Se(IV) (Doran, 1982; Maiers et al., 1988; Losi and Frankenberger, 1997; Kashiwa et al., 2000).

Selenite is often more toxic than the other forms of selenium, and organisms typically tolerate higher concentrations of selenate (Tomei et al., 1995; Kashiwa et al., 2000), although the relative order of toxicity can be species-specific (Coffmann et al., 1997). The transformation of selenite to reduced forms of selenium, under both aerobic and anaerobic conditions, is often thought to be a detoxification reaction (Oremland, 1994; Milne, 1998). In experiments where cell suspensions of *B. cepacia* were incubated with Se(IV), the solutions rapidly turned red, indicating the formation of the elemental Se(0). Therefore, it is possible that Se(IV) buildup occurs in biofilms amended with SeO_4^{2-} due to Se(IV) toxicity (Switzer-Blum et al., 1998), effectively shutting down further reduction of selenium oxoanions to Se(0).

However, we suggest that there may be a minimum threshold concentration for the efficient reduction of Se(IV). A greater fraction of Se(IV) intermediates are retained at the alumina surface in biofilm/alumina samples amended with low Se(VI) concentrations (i.e., the fraction of total Se in the Se(IV) form follows the sequence $10^{-5} > 10^{-4} > 10^{-3}$ M initial [SeO_4^{2-}] when the biofilms/alumina samples are incubated with SeO_4^{2-}, see Fig. 3C). These data suggest that when selenite is produced from the reduction of low concentrations of selenate, the Se(IV) concentrations are too low for significant conversion to Se(0). In addition, we note that selenite reduction was much greater at 10^{-3} M SeO_3^{2-} than at lower Se(IV) concentrations (Fig. 3B). Van Fleet-Stalder et al. (2001) noted that selenium uptake and transformation were much greater at 100 ppm than 1 ppm for *Rhodobacter sphaeroides*, which may be similar to the scenario presented here. Because we cannot detect the Se(IV) in the solution phase, it is possible that the Se(IV) concentration is often too low for the further reduction to Se(0), especially due to likely rapid, preferential binding of Se(IV) to the underlying alumina surface.

Visual observation that *B. cepacia* cell suspensions turn red after incubation with Se(IV) suggests that some fraction of the elemental Se is in the form of the red, amorphous allotrope. We did not monitor whether or not the red Se(0) converted to hexagonal, gray Se(0) over time. The distribution of the selenium particles (i.e., intracellular vs. extracellular or location within the biofilms) is unknown. Selenocysteine was not found in the fitting of any of the XANES spectra, and selenomethionine only comprised a significant fraction of the fit for the "residual" XANES spectrum for 10^{-3} M SeO_4^{2-} (Fig. 6), where the sample was comprised of only reduced forms of selenium after equilibration with Se-free solutions. These findings are in contrast to XANES spectra presented by de Souza et al. (2001), where aerobic, Se(VI) treated bacterial isolates accumulated Se(VI) and a selenomethionine-like species, but no selenite or Se(0). However, many other studies have found Se(0) to be the major product of selenium reduction (Oremland et al., 1989; Lortie et al., 1992; Tomei et al., 1992; Buchanan et al., 1995; Tomei et al., 1995; Garbisu et al., 1996; Losi and Frankenberger, 1998; Van Fleet-Stalder et al., 2000; Roux et al., 2001), similar to this study. The mechanism of selenium reduction may be nonspecific, such as reduction by numerous intracellular reductants after Se uptake into the cells, or by the activity of enzymes such as nitrate and nitrite reductases. Because all of the incubations with selenium were conducted after the cells were removed from growth solutions, the reduction capacity will be limited, and any specific activity is likely due to constitutive enzymes.

Optimal Se reduction conditions reported for many isolates typically fall within the range of near-neutral to alkaline pH (e.g., pH 6–9), whereas our experiments were conducted at pH 4.5. We did incubate *B. cepacia* cell suspensions with 10^{-4} M SeO_3^{2-} and SeO_4^{2-} at both pH 4.5 and pH 7 and measured comparable amounts of Se uptake for each experiment, although the fraction reduced was greater at pH 7. Therefore, we chose pH 4.5 as an appropriate pH to compare the role of sorption processes (anion sorption should be near maximum at the alumina surface) to bioreduction processes in the partitioning behavior of Se. Lower pH would not be physiologically relevant for *B. cepacia*, and at alkaline pH, sorption is expected to be significantly reduced.

5. CONCLUSIONS

The XSW technique allowed us to characterize the spatial distribution of selenium perpendicular to the interface between microbial biofilms and the α-Al_2O_3 (1-102) surface. These data can then be coupled with grazing incidence XANES spectra on the same samples to determine the speciation of Se at the alumina surface vs. in the biofilm. In particular, the spectroscopic data can be used to correlate changes in the Se partitioning behavior over time with the microbial reduction of selenium oxoanions.

The partitioning behavior of selenate, selenite, and elemental selenium differs markedly in the *B. cepacia* biofilms formed on α-Al_2O_3 (1-102) surfaces. Our data for Se(VI) partitioning behavior show that although Se uptake may be significant, Se(VI) is only weakly associated with the biofilm and the alumina surface, and the Se(VI) sorption complexes are easily remobilized, without requiring significant changes in ionic strength or pH. In contrast, selenite is strongly partitioned to reactive sites on the underlying alumina surfaces. When Se(IV) is generated as an intermediate during Se(VI) reduction to Se(0), some fraction of the Se(IV) is released from the biofilm and binds to the alumina surface, leading to large changes in the selenium partitioning behavior. The mechanism of Se(VI) and Se(IV) reduction to Se(0) is unknown, although the X-ray treated cells vs. active cells experiments demonstrate that reduction is biologically mediated, and ultimately the elemental Se that is produced is immobilized within the biofilm. Because aerobic conditions are maintained during the experiments (i.e., Se(VI) is the thermodynamically stable oxidation state), we infer that the bioreduction of Se(VI) and Se(IV) is a detoxification reaction that will eventually be limited by cell death or the availability of intracellular reductants. The bioavailability of the Se(IV) intermediates that sorb to the alumina surface is also unknown.

Selenate immobilization in soils is often attributed to the generation of elemental Se rather than sorption processes (Lucas and Hollibaugh, 2001), but the potential accumulation of Se(IV) intermediates at metal-(hydr)oxide surfaces may be significantly underestimated. In soil studies, reduction of selenate has been shown to be fast enough to produce selenite in the effluent and to leave elemental Se in the soil profile (Guo et al., 1999). The data from this study suggest that the selenite intermediates may be partially immobilized by sorption onto adjacent metal-(hydr)oxide surfaces, even when selenite cannot be measured in the overlying solutions. Therefore, the production of both Se(0) and Se(IV), which apparently can occur under aerobic, microaerophilic, and anaerobic conditions, will generate a large net sink for Se in environments with elevated selenate concentrations.

Acknowledgments— This work was supported by the National Science Foundation (NSF-EAR-9905755 and NSF-CHE-0089215) and the Eugene Holman Stanford Graduate Fellowship (AST). We appreciate the assistance provided by John Bargar, Joe Rogers, and the Biotech staff at the Stanford Synchrotron Radiation Laboratory (SSRL). SSRL is funded by the Department of Energy (Offices of Basic Energy Sciences and Biologic and Environmental Research) and by the National Institutes of Health. We also thank Scott Fendorf, Craig Criddle, Patricia Maurice (AE), and three anonymous reviewers for constructive input regarding this manuscript.

Associate editor: P. Maurice

REFERENCES

Abruna H. D., Bommarito G. M., and Acevedo D. (1990) The study of solid/liquid interfaces with X-ray standing waves. *Science* **250**, 69–74.

Balistrieri L. S. and Chao T. T. (1987) Selenium adsorption by goethite. *J. Soil Sci. Soc. Am.* **55**, 1145–1151.

Bedzyk M. J., Bommarito G. M., Caffrey M., and Penner T. L. (1990) Diffuse-double layer at a membrane-aqueous interface measured with X-ray standing waves. *Science* **248**, 51–56.

Bommarito G. M., White J. H., and Abruna H. D. (1990) Electrosorption of iodide on platinum: Packing density and potential-dependent distributional changes observed in-situ with X-ray standing waves. *J. Phys. Chem.* **94**, 8280–8288.

Brennan S. and Cowan P. L. (1992) A suite of programs for calculating x-ray absorption, reflection, and diffraction performance for a variety of materials at arbitrary wavelengths. *Rev. Sci. Instr.* **63**, 850–853.

Buchanan B. B., Bucher J. J., Carlson D. E., Edelstein N. M., Hudson E. A., Kaltsoyannis N., Leighton T., Lukens W., Shuh D. K., Nitsche H., Reich T., Robets K., Torretto P., Woicik J., Yang W. S., Yee A., and Yee B. C. (1995) A XANES and EXAFS investigation of the speciation of selenite following bacterial metabolization. *Inorg. Chem.* **34**, 1617–1619.

Coffmann Y. R., VanFleet-Stalder V., and Chasteen T. G. (1997) Toxicity of oxyanions of selenium and of a proposed bioremediation intermediate, dimethyl-selenone. *Environ. Tox. Chem.* **16**, 141–145.

Davis J. A. and Kent D. B. (1990) Surface complexation modeling in aqueous geochemistry. In *Mineral-Water Interface Geochemistry, Vol. 23* (eds. M. F. Hochella and A. F. White), pp. 177–260. Mineralogical Society of America, Washington, D.C.

de Boer D. K. G. (1991) Glancing-incidence X-ray fluorescence of layered materials. *Phys. Rev. B* **44**, 498–511.

de Souza M. P., Dojka M. A., Pickering I. J., Dawson S. C., Pace N. R., and Terry N. (2001) Identification and characterization of bacteria in a selenium-contaminated hypersaline evaporation pond. *Appl. Environ. Microbiol.* **67**, 3785–3794.

Doran J. W. (1982) Microbial organisms and the biological cycling of selenium. *Adv. Microb. Ecol.* **6**, 1–32.

Foster A. L. (1999) Partitioning and transformation of arsenic and selenium in natural and laboratory systems. Ph.D. thesis, Department of Geological & Environmental Sciences, Stanford University, Stanford, CA.

Foster A. L., Brown G. E. Jr, and Parks G. A. (2003) XAFS study of As(V) and Se(IV) sorption complexes on hydrous Mn oxides. *Geochim. Cosmochim. Acta* **67***(11)*, 1937–1953.

Frankenberger W. T. J. and Benson S. B. (1994) *Selenium in the Environment.* Marcel-Dekker. 456 pp.

Frankenberger W. T. J. and Engberg R. A. (1998) *Environmental Chemistry of Selenium.* Marcel-Dekker. 713 pp.

Garbisu C., Ishii T., Leighton T., and Buchanan B. B. (1996) Bacterial reduction of selenite to elemental selenium. *Chem. Geol.* **132***(1–4)*, 199–204.

George G. N. and Pickering I. J. (1995) EXAFSPAK, A suite of computer programs for the analysis of x-ray absorption spectra. Stanford Synchrotron Radiation Laboratory, Stanford, CA.

Guo L., Frankenberger W. T., and Jury W. A. (1999) Evaluation of simultaneous reduction and transport of selenium in saturated soil columns. *Water Resources Res.* **35***(3)*, 663–669.

Hayes K. F., Roe A. L., Brown G. E. Jr, Hodgson K. O., Leckie J. O., and Parks G. A. (1987) In-situ x-ray absorption study of surface complexes: Selenium oxyanions on α-FeOOH. *Science* **238**, 783–786.

Ike M., Takahashi K., Fujita T., Kashiwa M., and Fujita M. (2000) Selenate reduction by bacteria isolated from aquatic environment free from selenium contamination. *Water Resources Res.* **34**, 3019–3025.

Kashiwa M., Nishimoto S., Takahashi K., Ike M., and Fujita M. (2000) Factors affecting soluble selenium removal by a selenate-reducing bacterium *Bacillus sp SF-1*. *J. Biosci. Bioeng.* **89**, 528–533.

Kessi J., Ramuz M., Wehrli E., Spycher M., and Bachofen R. (1999) Reduction of selenite and detoxification of elemental selenium by the

phototrophic bacterium *Rhodospirillum rubrum*. *Appl. Environ. Microbiol.* **65**, 4734–4740.

Krol A., Sher C. J., and Kao Y. H. (1988) X-ray fluorescence of layered synthetic materials with interfacial roughness. *Phys. Rev. B* **38**, 8579–8592.

Lortie L., Gould W. D., Rajan S., McCready R. G. L., and Cheng K. J. (1992) Reduction of selenate and selenite by a *Pseudomonas stutzeri* isolate. *Appl. Environ. Microbiol.* **58**, 4043–4044.

Losi M. E. and Frankenberger W. T. J. (1997) Reduction of selenium by *Enterobacter cloacae* SLD1a-1: Isolation and growth of the bacterium and its expulsion of selenium particles. *Appl. Environ. Microbiol.* **63**, 3079–3084.

Losi M. E. and Frankenberger W. T. J. (1998) Reduction of selenium oxyanions by *Enterobacter cloacae* strain SLD1a-1. In *Environmental Chemistry of Selenium* (eds. W. T. J. Frankenberger and R. A. Engberg), pp. 515–544. Marcel-Dekker.

Lucas F. S. and Hollibaugh J. T. (2001) Response of sediment bacterial assemblages to selenate and acetate amendments. *Environ. Sci. Tech.* **35**, 528–534.

Macy J. M., Michel T. A., and Kirsch D. G. (1989) Selenate reduction by a *Pseudomonas sp.*: A new mode of anaerobic respiration. *FEMS Microbiol. Lett.* **61**, 195–198.

Maiers D. T., Wichlacz P. L., Thompson D. L., and Bruhn D. F. (1988) Selenate reduction by bacteria from a selenium-rich environment. *Appl. Environ. Microbiol.* **54**, 2591–2593.

Milne J. B. (1998) The uptake and metabolism of inorganic selenium species. In *Environmental Chemistry of Selenium* (eds. W. T. J. Frankenberger and R. A. Engberg), pp. 459–478. Marcel-Dekker.

Myeni S. C. B., Tokunaga T. K., and Brown G. E. Jr. (1997) Abiotic selenium redox transformations in the presence of Fe(II,III) oxides. *Science* **278**, 1106–1109.

Neal R. H. and Sposito G. (1989) Selenate adsorption on alluvial soils. *J. Soil Sci. Soc. Am.* **53**, 70–74.

Oremland R. S. (1994) Biogeochemical transformations of selenium in anoxic environments. In *Selenium in the Environment* (eds. W. T. J. Frankenberger and S. Benson), pp. 389–420. Marcel-Dekker.

Oremland R. S., Blum J. S., Culbertson C. W., Visscher P. T., Miller L. G., Dowdle P., and Strohmaier F. (1994) Isolation, growth, and metabolism of an obligately anaerobic, selenate-respiring bacterium, strain SES-3. *Appl. Environ. Microbiol.* **8**, 3011–3019.

Oremland R. S., Hollibaugh J. T., Maerst A. S., Presser T. S., Miller L. G., and Culbertson C. W. (1989) Selenate reduction to elemental selenium by anaerobic bacteria in sediments and culture: Biogeochemical significance of a novel, sulfate-independent respiration. *Appl. Environ. Microbiol.* **55**, 2333–2343.

Parratt L. G. (1954) Surface studies of solids by total reflection of X-rays. *Phys. Rev.* **95**, 359–369.

Pickering I. J., Brown G. E. Jr, and Tokunaga T. K. (1995) Quantitative speciation of selenium in soils using x-ray absorption spectroscopy. *Environ. Sci. Tech.* **29**, 2456–2459.

Pickering I. J., Prince R. C., and George G. N. (2000) Quantitative, chemically specific imaging of selenium transformation in plants. *Proc. Natl. Acad. Sci.* **97**, 10717–10722.

Roux M., Sarret G., Pignot-Paintrand I., Fontecave M., and Coves J. (2001) Mobilization of selenite by *Ralstonia metallidurans* CH34. *Appl. Environ. Microbiol.* **67**, 769–773.

Su C. M. and Suarez D. L. (2000) Selenate and selenite sorption onto iron oxides: An infrared and electrophoretic study. *Soil Sci. Soc. Am. J.* **64**, 101–111.

Switzer-Blum J., Burns-Bindi A., Buzzelli J., Stolz J. F., and Oremland R. S. (1998) *Bacillus arsenicolseneatis*, sp. nov., and *Bacillus selenitireducens*, sp. nov: Two haloalkaliphiles from Mono Lake, California that respire oxyanions of selenium and arsenic. *Arch. Microbiol.* **171**, 19–30.

Templeton A. S., Trainor T. P., Spormann A. M., Traina S. J., and Brown G. E. Jr. (2001) Pb(II) distributions at biofilm-metal oxide interfaces. *Proc. Natl. Acad. Sci.* **98,** *21,* 11897–11902.

Terry N. and Zayed A. M. (1994) Selenium volatilization by plants. In *Selenium in the Environment* (eds. W. T. J. Frankenberger and S. M. Benson), pp. 343–368. Marcel-Dekker.

Tokunaga T. K., Pickering I. J., and Brown G. E. Jr. (1996) Selenium transformations in ponded sediments. *Soil Sci. Soc. Am. J.* **60**, 781–790.

Tomei F. A., Barton C. L., Lemanski C. L., and Zocco T. G. (1992) Reduction of selenate and selenite to elemental selenium by *Wolinella succinogenes*. *Can. J. Microbiol.* **38**, 1328–1333.

Tomei F. A., Barton L. L., Lemanski C. L., Zocco T. G., Fink N. H., and Sillerud L. (1995) Transformation of selenate and selenite to elemental selenium by. *Desulfovibrio-desulfuricans. J. Ind. Microbiol.* **14**, 329–336.

Trainor T. P. (2001) X-ray scattering and x-ray absorption studies of the structure and reactivity of aluminum oxide surfaces. Ph.D. thesis, Department of Geological & Environmental Sciences, Stanford University, Stanford, CA.

Trainor T. P., Eng. P. J., Brown G. E. Jr, Robinson I. K., and De Santia M. (2002a) Crystal truncation rod diffraction study of the α-Al_2O_3 (1-102) surface. *Surf. Sci.* **496**, 238–250.

Trainor T. P., Templeton A. S., Brown G. E. Jr, and Parks G. A. (2002b) Application of the long period x-ray standing wave technique to the analysis of surface reactivity: Pb(II) sorption at α-Al_2O_3/aqueous solution interfaces in the presence and absence of Se(VI). *Langmuir* **18**, 5782–5791.

Turner R. J., Weiner J. H., and Taylor D. E. (1998) Selenium metabolism in *Escherichia coli*. *Biometals* **11**, 223–227.

Van Fleet-Stalder V., Chasteen T. G., Pickering I. J., George G. N., and Prince R. C. (2000) Fate of selenate and selenite metabolized by *Rhodobacter sphaeroides*. *Appl. Environ. Microbiol.* **66***(11),* 4849–4853.

Zhang P. C. and Sparks D. L. (1990) Kinetics of selenate and selenite adsorption desorption at the goethite-water interface. *Environ. Sci. Tech.* **24,** *12,* 1845–1856.